

A Study of Dense Suspensions Climbing Against Gravity

Xingjian Hou and Joseph D. Peterson

*DAMTP, Centre for Mathematical Sciences, University of Cambridge, CB3 0WA,
United Kingdom*

Abstract

Dense suspensions have previously been shown to produce a range of anomalous and gravity-defying behaviors when subjected to strong vibrations in the direction of gravity. These behaviors have previously been interpreted in terms of rigid body phenomena and shear-thickening, but here we examine discontinuous shear thickening (DST) as the cause of a “negative viscosity” effect, i.e. the average shear rate being opposite to the direction of the average shear stress. Using ideas from the Wyart and Cates modeling framework, we show that such a “negative viscosity” can be achieved in shear flows driven by oscillating stress with both square and sinusoidal wave forms. We extend this same modeling approach to study falling films in a vibrating gravitational field, where we similarly find it is possible to attain an overall flow opposite the direction of gravity. Preliminary experimental findings are also provided in support of the modeling work.

1 Introduction

A dense suspension is a suspension of solid particles in fluid, with particle density high enough that the rheological properties are dominated by the system’s proximity to a “jamming” transition. Dense suspensions are found in applications ranging from construction to comestibles, and their ubiquity arises in part due to the difficulty of transporting dry powders - dense suspensions do not generate dust, they do not cake, and they are less susceptible to flow-induced segregation effects. Besides their relative ease of processing, high density particulate loading can also improve the viscosity/texture of fluids like paint and toothpaste.

In dense suspensions, the proximity of a system to jamming is sensitive to the details of inter-particle interactions - any interaction that removes degrees of freedom from the relative motion of two particles will bring the system closer to jamming [1]. Practically speaking, one is most often concerned with a distinction between “sliding contacts” and “frictional contacts”, where the latter has fewer degrees of freedom. In recent years, there has been growing interest in tuning/controlling the rheological properties of a dense suspension by applying vibrations that manipulate the relative proportion of sliding and frictional contacts [2]. In particular, it has been found that vibrations transverse to the direction of flow can disrupt the formation of frictional contacts and mitigate the risk of flow-induced jamming for systems at very high particle loadings [3].

Vibrations parallel to flow have received comparatively little attention, but vertically vibrated dense suspensions (VVDS) - in which vibrations are applied parallel to gravity - are an active area of research. Previous experiments have shown that Faraday waves and persistent holes can occur at the surface of VVDS [4], and with increasing acceleration more complex structures emerge, including features described as rivers, fingers, and jumping liquids [5]. Shinbrot et al [6] have also studied a similar problem, in which dense suspensions showed “climbing” behaviors in the presence of a vertically vibrating probe.

In all the aforementioned phenomena, the suspensions exhibit a tendency to move up/maintain shapes against the influence of gravity. In the solid mechanics literature, there is some precedent for vertical vibrations favoring motion against gravity (e.g. the inverted vibrating pendulum [7]). Some authors have attempted to extend this analogy for interpreting the behavior of VVDS [8], but this explanation fails to account for the fundamentally fluid-like character of the material. For Newtonian fluids, there is also precedent for vertical vibrations favoring motion against gravity [9], where an interplay between inertial and capillary forces allows isolated droplets to climb up a partially inclined surface. However, this climbing mechanism does not apply to behaviors seen in bulk VVDS, nor does it permit climbing on surfaces fully inclined to 90° . For ordinary shear thickening fluids, Deegan [10] proposed a “ratcheting mechanism” to explain climbing behaviors in terms of discontinuous shear thickening and stress hysteresis in the underlying flow curve. Later simulation work by Shinbrot et al [6] also suggested that a similar ratcheting mechanism might occur for fluids climbing up a vertically vibrating probe, though it is curious that the simulations by Shinbrot et. al. only required continuous shear thickening. Comparing the ideas from Deegan et. al. and Shinbrot et. al. we suggest that the source of vibrations (vibrating platform vs vibrating external probe) may play a more important role than one might initially expect.

For a general explanation of climbing behaviors in VVDS, the ratcheting mechanism proposed by Deegan to be most promising, and in this paper we provide follow-up analysis to (1) directly connect the mechanism to changes in inter-particle contacts and (2) generalize the “ratcheting” idea to the more generic notion of “negative apparent viscosity”. These ideas will be supported by calculations from the Wyart and Cates (WC) modeling framework and new, unambiguous evidence of sustained “climbing” behavior in VVDS.

The organization of our paper is as follows: Section 2 outlines the methods of our study, including both the equations the motion for the Wyart-Cates (WC) theory [1] (section 2.1) and describes the setup of a proof-of-principle experiment (section 2.2). Section 3 presents calculations, using the WC model, for average shear rate under oscillating shear stress (sections 3.1 and 3.2) and average flow rate in a falling film under oscillating gravity (sections 3.3 and 3.4). We also provide a limited discussion on the effect of finite inertia (section 3.5). Section 4 describes the results of our experimental efforts, including both replicated results from past experiments and the new observation of climbing droplets. The new results are discussed in relation to the predictions from section 3. Section 5 summarizes the results of our study and suggests directions for future research.

2 Methods

In this paper, we aim to demonstrate how discontinuous shear thickening (DST) can account for the gravity-defying behavior of dense suspensions. To achieve this, we require a modeling tool that relates rheology to the fluid microstructure, is large in scale compared to particle size (i.e. continuum models), is suitable for reversing flows, and has minimal complexity. The Wyart-Cates (WC) model satisfies all conditions except for fluid reversal, but alternative models suited to flow-reversal have higher complexity [11]. We also note that the concerns about reversing flows can be mitigated when the reversing strain amplitude is large in comparison to the strain required for re-organization of the microstructure. In any case, we will defer to using WC as the less complex model for a first study.

In our experimental efforts, we will aim to conduct proof-of-principle tests for the basic model predictions, and also provide some new experimental results that more unambiguously isolate the “climbing” behavior of VVDS. Future experimental efforts in this vein will require more precise equipment for a systematic study.

The subsections that follow provide a more complete description of the modeling

and experimental tools that support the results in sections 3 and 4.

2.1 Theory

From the Wyart-Cates model, the steady stress-strain rate relationship of dense suspensions in simple shear flow is given by:

$$\begin{aligned}\sigma &= \eta \dot{\gamma}, \eta = \frac{\eta_0}{(\phi - \phi_J)^2}, \\ \phi_J &= f \phi_R + (1 - f) \phi_S, \\ f &= \exp\left(-\frac{\sigma^*}{\Pi}\right)\end{aligned}\tag{1}$$

where $\dot{\gamma}$ is the shear rate of the suspension, σ is the shear stress on the suspension, $\Pi = \text{tr}(\mathbf{\Sigma}/3)$ is the particle pressure with $\mathbf{\Sigma}$ being the particle stress tensor (note that σ denotes the xy component of $\mathbf{\Sigma}$). For steady simple shear flow, the particle pressure $\Pi = \text{tr}(\mathbf{\Sigma}/3)$ should be positive and proportional to the shear stress $\Pi \propto |\sigma|$, and for our purposes the constant of proportionality can be absorbed into the choice of σ^* , which is the critical stress needed to drive particles into contact. For a given fraction of frictional contacts, f , Eq. 1 prescribes a jamming fraction ϕ_J that interpolates linearly between the jamming fraction for purely sliding constraints, ϕ_S , and purely rolling constraints, ϕ_R . Note that f is a function of the scaled particle pressure $|\sigma|/\sigma^*$, with frictional contacts being favored for large particle pressures. For the purpose of this paper, we will assume $\phi_R = 0.57$, $\phi_S = 0.64$. The viscosity of the suspension η is related to the actual volume fraction of the suspension ϕ . The pre-factor in the Krieger–Dougherty equation [12] is denoted by η_0 and is proportional to the viscosity of the suspending fluid. For further discussions, we refer the readers to the original paper by Wyart and Cates [1].

The principal success of the WC model is its ability to qualitatively capture a progression from continuous shear thickening (CST) to discontinuous shear thickening (DST) and shear jamming (SJ) with increasing particle volume fraction. In Fig. 1, we plot example “flow curves” for the shear stress σ as a function of the shear rate $\dot{\gamma}$ over a range of volume fractions ϕ covering this transition. Given the assumed values $\phi_R = 0.57$, $\phi_S = 0.64$, the WC model predicts that hysteresis and DST occur in the range $0.555 < \phi < 0.64$. For $0.57 \leq \phi < 0.64$, it is possible for SJ to occur, i.e. obtaining $\dot{\gamma} = 0$, once σ exceeds a critical value. For $\phi < 0.555$, only CST is observed.

Where the shear stress is known, Eq. 1, can be used to determine the corresponding shear rate:

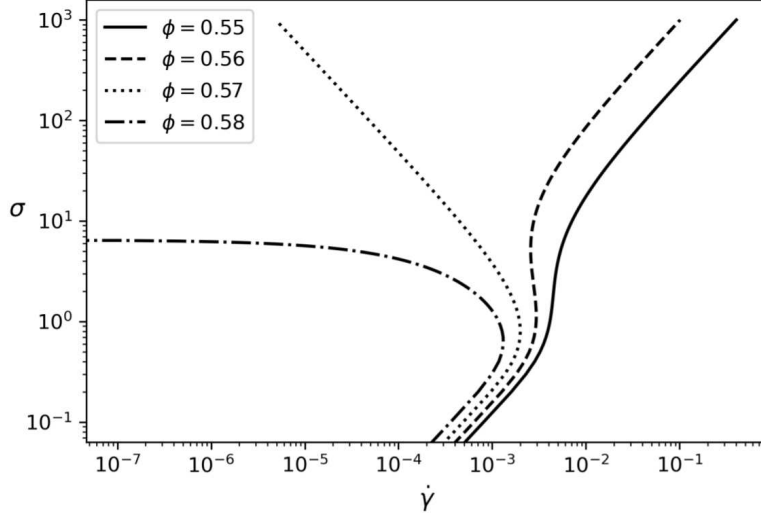


Figure 1: Predictions from the Wyart and Cates (WC) model (Eq. 1) for the steady shear stress σ as a function of shear rate $\dot{\gamma}$ for particle volume fractions $\phi = 0.55, 0.56, 0.57, 0.58$, assuming WC parameters $\phi_R = 0.57, \phi_S = 0.64, \sigma^* = 1, \eta_0 = 1$.

$$\dot{\gamma} = \begin{cases} \frac{\sigma}{\eta_0} \left[(\phi_R - \phi_S) \exp\left(-\frac{\sigma^*}{|\sigma|}\right) + (\phi_S - \phi) \right]^2, & \phi < \phi_J \\ 0, & \phi > \phi_J \end{cases} \quad (2)$$

Eq. 2 can also be generalized for a known time-dependent shear stress, $\sigma(t) = \sigma_0 + \Delta\sigma(t)$. For a forcing that's periodic on time T , we can define an average shear rate $\bar{\dot{\gamma}}$ by:

$$\bar{\dot{\gamma}} = \frac{1}{T} \int_0^T dt \dot{\gamma}(t) \quad (3)$$

Likewise, we can define a cycle-averaged viscosity $\bar{\eta} = \sigma_0 / \bar{\dot{\gamma}}$, assuming $\Delta\sigma(t)$ has zero mean. For Newtonian fluids - and indeed for most non-Newtonian fluids, the sign of $\bar{\eta}$ is always positive. However, our calculations in sections 3.1 and 3.2 suggest that this may not always be the case for dense suspensions.

The coupling between fluid motion¹ and fluid stresses in a fluid film is determined by via the Navier-Stokes equation, conserving momentum:

¹For convenience, equation 4 is written in the frame of the solid boundary. In the lab frame the suspension is under constant gravity \mathbf{g}_0 and the solid boundary vibrates with acceleration $-\Delta\mathbf{g}(t)$ of period T and aligned with gravity, so the equivalent gravity is $\mathbf{g}(t) = \mathbf{g}_0 + \Delta\mathbf{g}(t)$ in the vibrating frame.

$$\rho\left(\frac{\partial \mathbf{u}}{\partial t} + \mathbf{u} \cdot \nabla \mathbf{u}\right) = -\nabla p + \nabla \cdot \boldsymbol{\sigma} + \rho \mathbf{g} \quad (4)$$

We also assume an incompressible flow:

$$\nabla \cdot \mathbf{u} = 0 \quad (5)$$

For uni-direction flow, $\mathbf{u} = u_x \mathbf{e}_x$. Assuming uniform pressure, Eq. (3) becomes:

$$\rho \frac{\partial u}{\partial t} = \frac{\partial \sigma}{\partial x} + \rho g_x \quad (6)$$

Eq. 6 will be applied to model oscillatory shear flows, $g_x = 0$, and falling films under oscillating gravity, $g_x = g_0 + \Delta g(t)$, where g_0 is normal gravity and $\Delta g(t)$ is a zero-mean oscillation.

For the remainder of this report, we will conduct our analysis in terms of non-dimensionalized equations. A set of characteristic scales is defined to non-dimensionalize Eq. (3). The time scale is $\tau_C = T$, the period of oscillation. The length scale is $y_c = H$, the thickness of the fluid film. We assign a stress scale σ_C on the basis of the average forcing: for flows driven by an oscillating shear stress $\sigma(t)$ of period T , we choose $\sigma_C = \sigma_0$, where $\sigma_0 = \frac{1}{T} \int_0^T dt \sigma(t)$ is the average shear stress. For falling film flow driven by oscillating gravity $g_x(t)$, we choose $\sigma_C = \sigma_0$ where $\sigma_0 = \rho g_0 H$ gives the wall shear stress for a Newtonian fluid under fixed gravity $g_0 = \frac{1}{T} \int_0^T dt g_x(t)$. Given these characteristic stresses, we consider the zero shear viscosity of the fluid $\eta_{\dot{\gamma}=0}$ to estimate a characteristic velocity, $u_C = H \sigma_C / \eta_{\dot{\gamma}=0}$. Rescaling all variables in this way, we obtain:

$$Re \frac{\partial}{\partial t} u = -\frac{g_x}{g_0} + \frac{\partial \sigma}{\partial x} \quad (7)$$

where:

$$Re = \left(\frac{H^2 \rho}{\eta_{\dot{\gamma}=0} T} \right) \quad (8)$$

$Re = H^2 \rho / T \eta_{\dot{\gamma}=0}$ is a dimensionless variable comparing the typical scale of inertial forces to viscous forces. For the purpose of study, we assume $Re \ll 1$, as we are interested in high viscosity fluids, $\eta_{\dot{\gamma}=0} \sim 1 Pa \cdot s$, small lengthscales, $H \sim 1 mm$, and modest cycle times, $T \sim 0.1 s$. The system is also influenced by (1) the typical stresses in the fluid relative to the stress required for frictional contact σ_0 / σ^* , where $\sigma_0 = \sigma_C$ for a fluid film; (2) the relative amplitude of the oscillations $\Delta \sigma / \sigma_0, \Delta g / g_0$, where $\Delta \sigma, \Delta g$ is the amplitude of the oscillations $\Delta \sigma(t)$ and $\Delta g(t)$.



Figure 2: Experimental setup: The loudspeaker and the digital amplifier connected to each other. A plastic container was adhered to the loudspeaker to contain the fluid. Experiments were conducted with the plastic container alone or with additional structures attached, including a plastic straw.

2.2 Experiments

In the experiment, an oscillating signal is generated via an online tone generator [13] connected to a digital amplifier (Lepy Lp 2020A). A loudspeaker (Pyle PLMR61B, 120W) connects to the amplifier, providing oscillation and containing the suspension. To contain the fluid, we adhered a plastic container (dimensions 10cm diameter, 4cm height) to the surface of the loudspeaker using hot-melt adhesive. Experiments were conducted with the plastic container alone or with additional structures attached, including (as seen in Fig. 2) a plastic straw (1.2 cm diameter, 20 cm height).

In the experiment, the frequencies of oscillations range between $1 \sim 25Hz$. At 10Hz, where many of our experiments were conducted, the maximum displacement was observed to be approximately 1cm, corresponding to an acceleration of $\Delta g = 40m/s^2$.

3 Modeling Results

In this section we will employ Eqs. 1 and 7 (with $Re = 0$) to model the effect of vibrations/oscillations parallel to the direction of flow, especially as it pertains to a cycle-averaged shear rate $\bar{\dot{\gamma}}$ (oscillating shear flows, sections 3.1 and 3.2) or a cycle-averaged flow rate (oscillating falling films, sections 3.3 and 3.4). Finally, in section 3.5, the effect of finite inertia on the motion of fluid film with sinusoidal forcing is discussed and it is found that a small amount of inertia gives a first correction term that averages to zero.

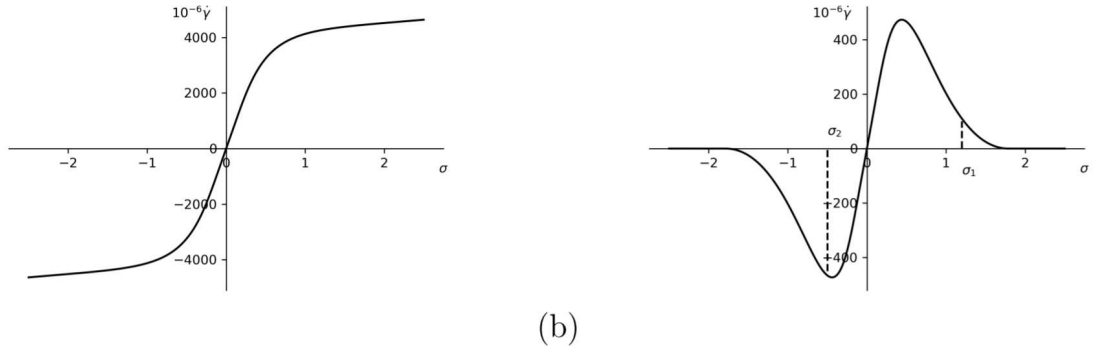


Figure 3: (a) Shear rate $10^{-6}\dot{\gamma}$ - stress σ relationship for suspension with $\phi = 0.55$. It is impossible to obtain σ_1, σ_2 such that $\sigma_1 + \sigma_2 > 0, \dot{\gamma}_1 + \dot{\gamma}_2 < 0$. (b) Shear rate $10^{-6}\dot{\gamma}$ - stress σ relationship for suspension with $\phi = 0.6$. It is possible to obtain σ_1, σ_2 such that $\sigma_1 + \sigma_2 > 0, \dot{\gamma}_1 + \dot{\gamma}_2 < 0$.

Before proceeding with detailed calculations, we first provide a general discussion on the underlying mechanism by which one might obtain an apparent negative viscosity from a dense suspension. Fig. 3(a) gives the flow curve for a sample CST fluid, $\phi = 0.55 < 0.555$. Here, shear rates always increase with increasing shear stress, and it is not possible to choose a set of points along the flow curve for which the average shear rate and the average shear stress do not have the same sign. However, for a DST fluid like that shown in Fig. 3(b), there is a portion of the flow curve where the shear stress is decreasing with increasing shear rate. Neglecting, for the moment, concerns over the stability of these portions of the flow curve, it is now possible to choose a pair of points (e.g. corresponding to the start of the high viscosity branch at positive shear rates and the end of the low viscosity branch at negative shear rates) such that the average shear rate $\bar{\dot{\gamma}} = (\dot{\gamma}_1 + \dot{\gamma}_2)/2$ corresponds to motion opposite direction to average shear stress $\sigma_0 = (\sigma_1 + \sigma_2)/2$, thus giving the appearance of a “negative viscosity”.

Before proceeding to detailed calculations, we acknowledge that there are at least two limitations to the mechanism as outlined above. First, the WC modeling framework only applies to steady flow calculations and performs poorly under reversing flow conditions. Therefore, our use of WC assumes that the strain-scale for the reversing flow is larger than the strain scale for microstructure re-organization. Second, the negatively-sloping portions of the WC flow-curve are essential to our proposed mechanism, but these are known to be unstable to (for example) vorticity banding instabilities. In this respect, our use of WC can be interpreted in one of two possible ways: (1) the strain scale for reversing flow is not large enough for instabilities to develop or (2) the basic hysteretic structure of the WC flow curve is more or less preserved even where a uniform

flow is not attainable. A more robust modeling study to validate this mechanism for a “negative viscosity” would require a fully tensorial and non-local constitutive equation, the likes of which has yet to be derived and validated for 3D flows at this time. Thus, we acknowledge the limitations of our modeling approach and we look forward to seeing these ideas tested more fully as constitutive modeling capabilities improve.

3.1 Square-wave Oscillations in Shear Stress

In this section, we will consider flow driven by a defined time-dependent shear stress following a square-wave variation in time:

$$\sigma(t) = \begin{cases} \sigma_0 + \Delta\sigma & \text{if } t \pmod{1} < 1/2 \\ \sigma_0 - \Delta\sigma & \text{if } t \pmod{1} \geq 1/2 \end{cases} \quad (9)$$

From Eq. 9, we see that shear stress alternates between $\sigma_1 = \sigma_0 + \Delta\sigma$ and $\sigma_2 = \sigma_0 - \Delta\sigma$ over equal time periods. The shear rate evolution over a period is shown in Fig. 4(a).

Fig. 4(b) shows average shear rates $\bar{\dot{\gamma}}$ under different $\sigma_0, \Delta\sigma$. Negative shear rates can only be achieved for $\Delta\sigma/\sigma_0 > 1$ as this is the minimum condition for any negative stress to appear at all. For higher $\Delta\sigma/\sigma_0$ and σ_0/σ^* however, there can be zero shear rate where the system is jammed.

As shown in Fig. 5, negative shear rates cannot occur for $\phi = 0.55 < 0.555$ without DST, while they can occur for $0.555 < \phi < 0.64$ with DST. For $0.57 < \phi < 0.64$, sufficiently large stresses are capable of inducing jamming, i.e. the total cessation of flow $\dot{\gamma} = 0$. With volume fractions approaching $\phi = 0.64$, negative shear rates occur over a wider range of stress protocols as the rheological contrast between frictional and frictionless flow is more pronounced.

3.2 Sine-wave Oscillations in Shear Stress

Square wave stress protocols are useful for introducing the idea of shear rates opposite to shear stresses in DST fluids, and here we show that the same mechanism extends (albiet less efficiently) to a flow driven by a sinusoidal stress protocol, $\sigma(t) = \sigma_0 + \Delta\sigma\sin(2\pi t)$. The stresses and shear rates at each moment are determined and the shear rates are averaged with Eq. 3.

As shown in Fig. 6, the sine wave stress protocol gives predictions similar to those observed in Fig. 4. Here, however, it is harder for negative average shear rates to

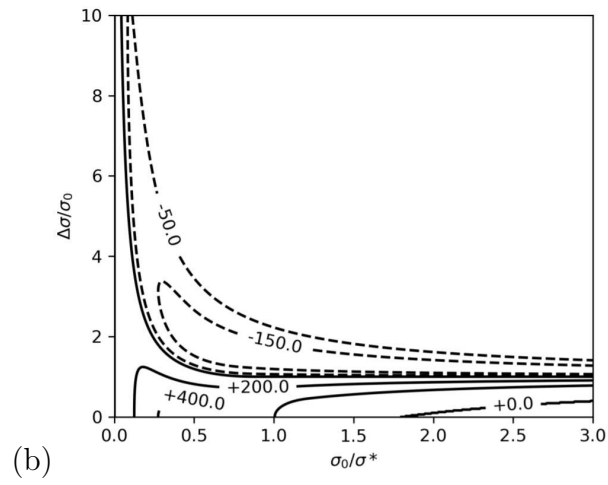
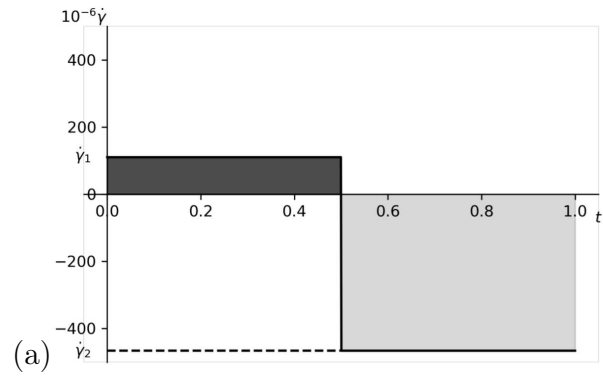


Figure 4: (a) Strain rate $10^{-6}\dot{\gamma}$ evolution of $\phi = 0.6$ over a period of square-wave stress with $\sigma_0/\sigma^* = 0.35$, $\Delta\sigma/\sigma_0 = 2.4$. (b) Average shear rates $10^{-6}\bar{\dot{\gamma}}$ of suspension of volume fraction $\phi = 0.6$ under square wave stresses of different average stresses σ_0/σ^* and oscillation amplitudes $\Delta\sigma/\sigma_0$.

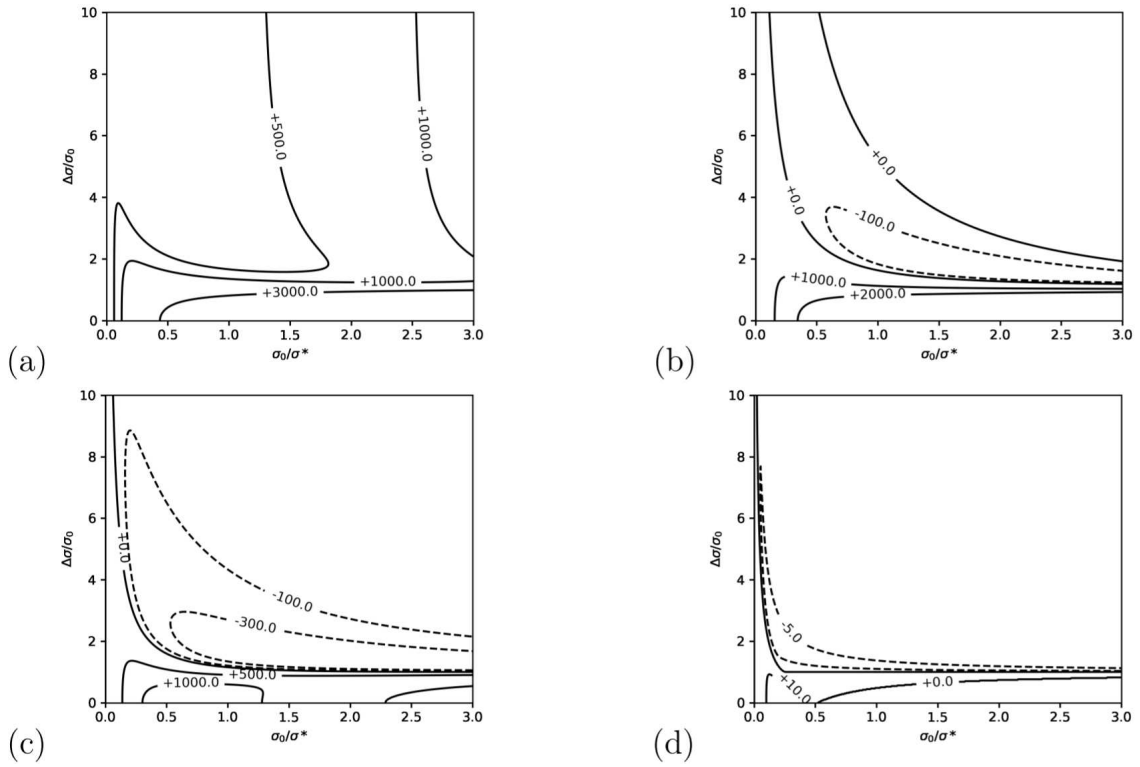


Figure 5: Average shear rates $10^{-6}\bar{\gamma}$ of suspensions of volume fractions ϕ : (a) 0.55 (b) 0.56 (c) 0.58 (d) 0.63 under square wave stresses of different average stresses σ_0/σ^* and oscillation amplitudes $\Delta\sigma/\sigma_0$.

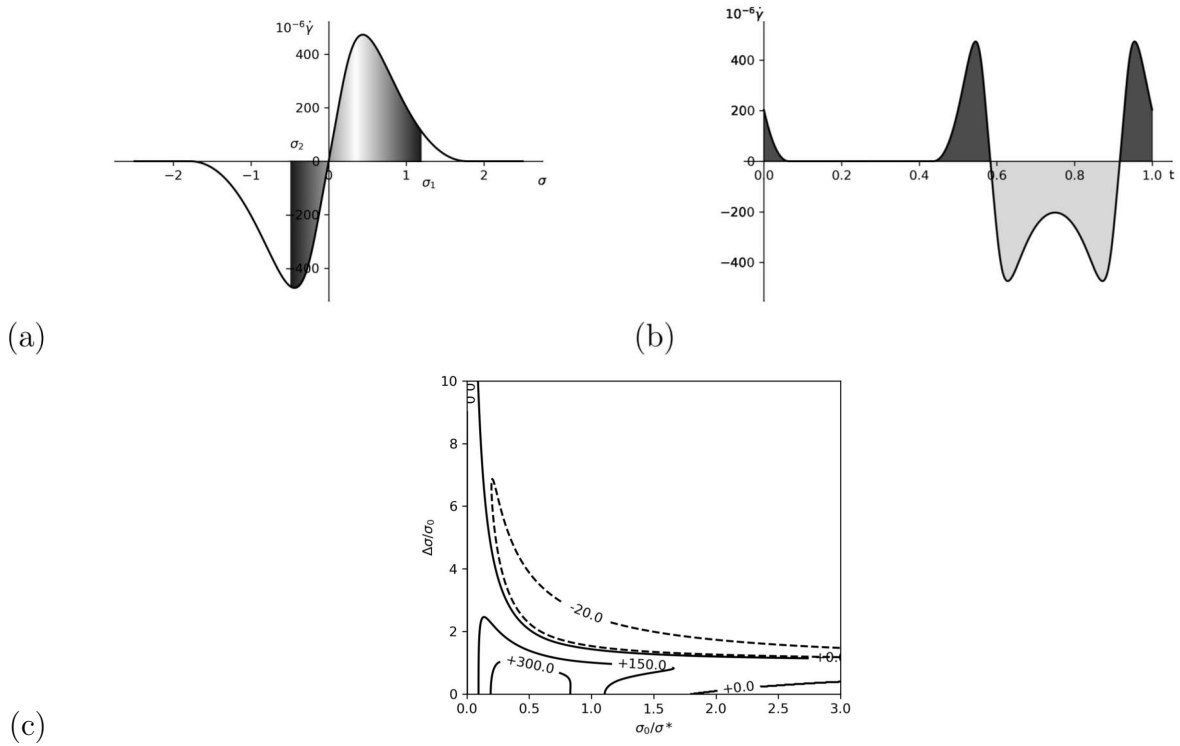


Figure 6: (a) The strain rate $10^{-6}\dot{\gamma}$ - stress σ relationship for suspension with $\phi = 0.6$. The color gradient demonstrates how much different stresses are weighted when averaging strain rates over a period. (b) The strain rate $10^{-6}\dot{\gamma}$ evolution over a period of sinusoidal stress with average stress $\sigma_0/\sigma^* = 1$, relative amplitude $\Delta\sigma/\sigma_0 = 2$. (c) Average shear rates $10^{-6}\bar{\dot{\gamma}}$ of suspension of volume fraction $\phi = 0.6$ under sinusoidal stresses of different average stresses σ_0/σ^* and relative amplitude $\Delta\sigma/\sigma_0$.

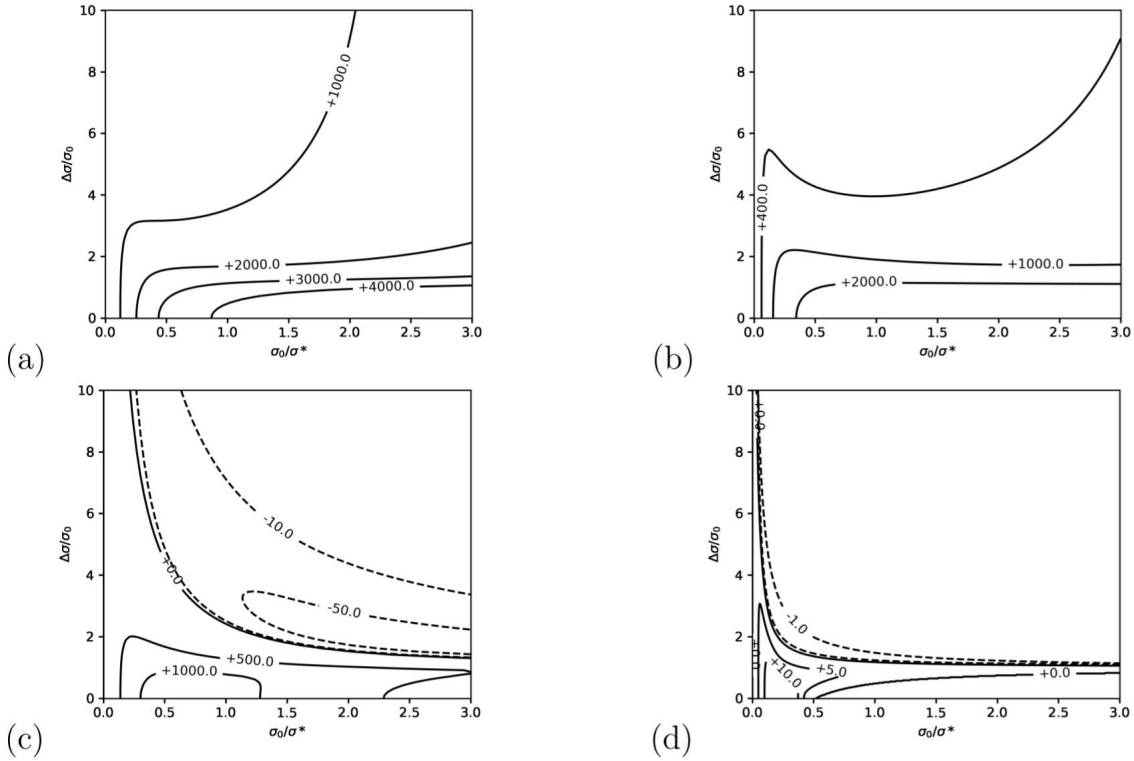


Figure 7: Average shear rates $10^{-6}\dot{\gamma}$ of suspensions of volume fractions ϕ : (a) 0.55 (b) 0.56 (c) 0.58 (d) 0.63 under sinusoidal stresses of different average stresses σ_0/σ^* and relative amplitudes $\Delta\sigma/\sigma_0$.

occur because the fluid spends more time exploring the non-inverted portions of the flow curve with high positive shear rates.

As shown in Fig. 7, negative shear rates can only be observed for $\phi > 0.57$ when the stress protocol is sinusoidal. This is a stricter requirement than the square wave, which only requires DST or $\phi > 0.555$. At high ϕ , the inverted portion of the flow curve is more extended, so large positive shear rates will be explored less by the fluid and it is easier to achieve negative average shear rates.

3.3 Square-wave Oscillations in Gravity

Simple shear flows driven by defined stresses are perhaps the most well-defined means of testing the premise of a “negative viscosity” in vibrated dense suspensions. In this subsection (and the one that follows) we turn our attention to predictions for falling films in oscillatory gravity. The basic premise is still the same: the strength of gravity controls the scale of stresses within the fluid, and the fluid moves faster under weak

(reversed) gravity than strong (normal) gravity.

In parallel to our analysis in section 3.1, we first consider the motion of the fluid film under a gravity following a square-wave variation in time:

$$g_x(t) = \begin{cases} g_0 + \Delta g & \text{if } t \pmod{1} < 1/2 \\ g_0 - \Delta g & \text{if } t \pmod{1} \geq 1/2 \end{cases} \quad (10)$$

The motion of the fluid film is described by Eq. 7. We first assume $Re \sim 0$, so:

$$1 \pm \frac{\Delta g}{g_0} = \frac{\partial \sigma}{\partial x} \quad (11)$$

Taking the free surface as $x = 0$, we have:

$$\sigma = \left(1 \pm \frac{\Delta g}{g_0}\right)x \quad (12)$$

which gives the shear stress at every position of the film $x \in [0, 1]$. The shear rates at each x position are determined from the corresponding shear stresses. The velocity is obtained through integrating shear rates:

$$v(x) = \int_0^x dx' \dot{\gamma}(t, x) + u(t) \quad (13)$$

where $u(t)$ is the velocity of the solid boundary, and over a period $\overline{u(t)} = 0$. Averaging $v(x)$ over each position $x \in [0, 1]$, we can obtain the velocity of the film:

$$\bar{u} = \int_0^1 dx u(t, x) \quad (14)$$

The average velocity over a period is obtained through Eq. 3. Similar to section 3.3, negative values can be obtained for $\Delta g/g_0 > 1$, which is the minimum condition for any stress to appear at all. However, Eq. 12 shows that part of the fluid is constantly under low stress, i.e., in the uninverted portions of the flow curve. This makes it harder to achieve negative \bar{u} as the positive shear rates are explored more by the fluid film.

3.4 Sine-wave oscillations in Gravity

In parallel with the results given in section 3.2, we now extend our analysis to fluid films with gravitational forcing varying sinusoidally in time, $g(t) = g_0 + \Delta g \sin(2\pi t)$. In the case of sine waves, Eqs. 11 and 12 are substituted with

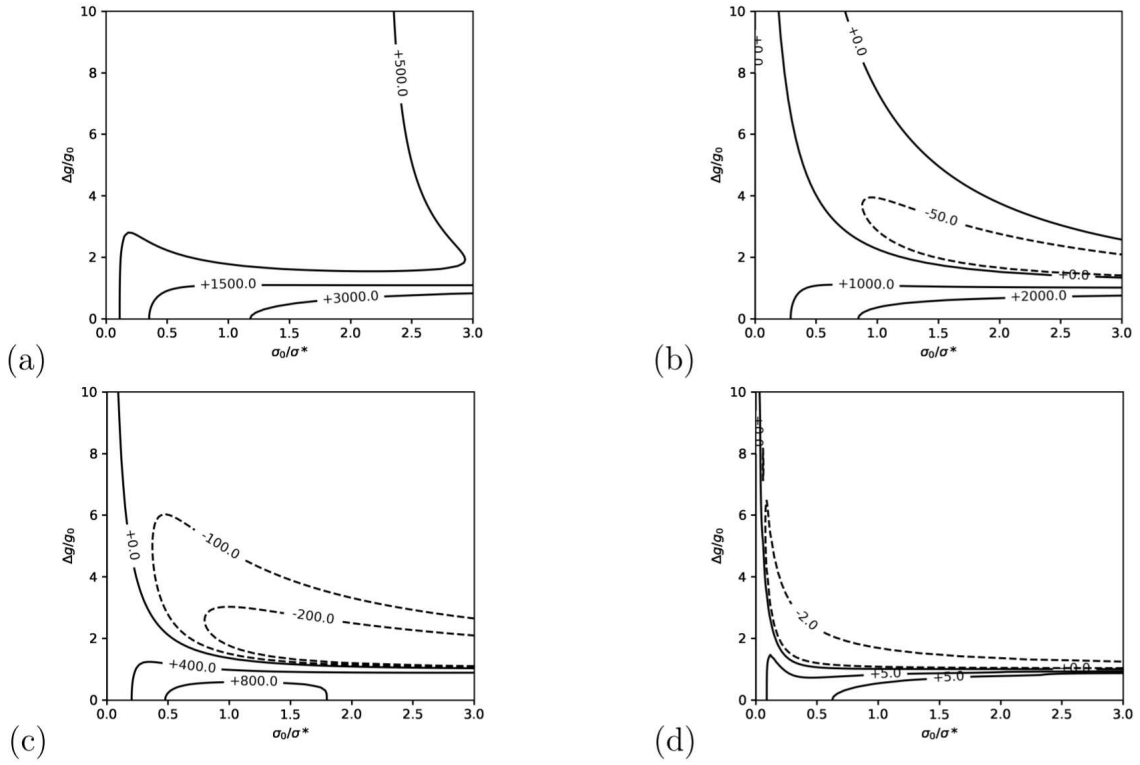


Figure 8: The velocities $10^{-6}\bar{u}$ of falling films of volume fractions ϕ : (a) 0.55 (b) 0.56 (c) 0.58 (d) 0.63 under square-wave gravity of different average stresses σ_0/σ^* (where $\sigma_0 = \rho g_0 H$) and relative amplitudes $\Delta g/g_0$.

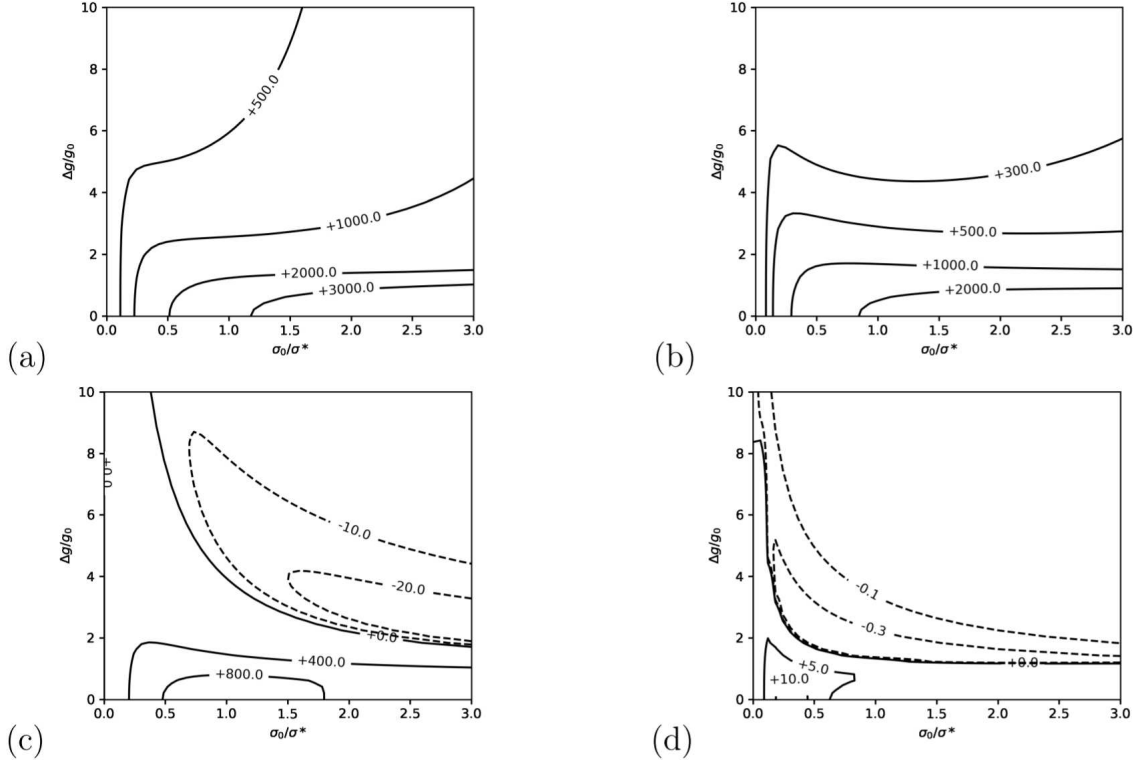


Figure 9: Velocities $10^{-6}\bar{u}$ of films of volume fractions ϕ : (a) 0.55 (b) 0.56 (c) 0.58 (d) 0.63 under sine-wave gravity of different average stresses σ_0/σ^* (where $\sigma_0 = \rho g_0 H$) and relative amplitudes $\Delta g/g_0$.

$$1 \pm \frac{\Delta g}{g_0} \cos(t) = \frac{\partial \sigma}{\partial x}, \sigma = [1 \pm \frac{\Delta g}{g_0} \cos(t)]x \quad (15)$$

The average velocity of the fluid film follows similar calculation procedure as in Eqs. 13 and 14. It is harder to achieve negative velocity than in both sections 3.2 and 3.3, as (1) similar to section 3.3, part of the film is constantly under low stress and (2) the gravity can fluctuate to lower values during oscillation, so the fluid will explore more the positive shear rates.

3.5 Some results for finite inertia

From Eqs. 7 and 8, the finite Reynolds number can be of influence to the fluid motion. In the experiments, $\eta_{\dot{\gamma}=0} \sim 1 Pa \cdot s, H \sim 1 mm, T \sim 0.1 s, \rho \sim 1000 kg/m^3$, so $Re \sim 0.01$. Here we consider the case of $Re < 1$ but being finite.

For section 3.4, we now consider the case of Re being small but finite.

Eq. (5) is now written as:

$$Re \frac{\partial}{\partial t} u = -(1 + \frac{\Delta g}{g_0} \cos(2\pi t)) + \frac{\partial \sigma}{\partial x} \quad (16)$$

Expanding $u(t), \sigma(t)$ with respect to Re :

$$\begin{aligned} u(Re, t) &= u_0(t) + u_1(t)Re + \dots, \\ \sigma(Re, t) &= \sigma_0(t) + \sigma_1(t)Re + \dots \end{aligned} \quad (17)$$

Plugging (13) into (12) we find:

$$0 = \left\{ - \left[1 + \frac{\Delta g}{g_0} \cos(2\pi t) \right] + \frac{\partial \sigma_0}{\partial x} \right\} Re^0 + \left\{ - \frac{\partial u_0}{\partial t} + \frac{\partial \sigma_1}{\partial x} \right\} Re^1 + \dots \quad (18)$$

The coefficients for each order of Re should be zero, so:

$$\frac{\partial \sigma_0}{\partial x} = 1 + \frac{\Delta g}{g_0} \cos(2\pi t), \quad (19)$$

$$\frac{\partial \sigma_1}{\partial x} = \frac{\partial u_0}{\partial t} \quad (20)$$

Eq. (15) is an even function about time $t = 1/4$, the same for the velocity $u_0(x, t)$ at any point x under low Re . This also means that $\partial_t u_0(x, t)$ is an odd function about time $t = 1/4$ for any x . So it must also be true that $\sigma_1(x, t) = \int_0^x da \partial_t u_0(a, t)$ is an odd function about $t = 1/4$, since it is just a sum of odd functions.

We also expand $\dot{\gamma}(t)$ with $\dot{\gamma}(Re, t) = \dot{\gamma}_0(t) + Re\dot{\gamma}_1(t) + \dots$. For low Re we have:

$$\dot{\gamma}_1 = \frac{\partial \dot{\gamma}}{\partial \sigma}(\sigma_0(x, t))\sigma_1 \quad (21)$$

Where the input to a function is even, then output must also be even, so $\frac{\partial \dot{\gamma}}{\partial \sigma}(\sigma_0(t, y))$ is an even function about time $t = 1/4$.

If we compute the average shear rate on a time $t \in [-1/4, 3/4]$, such that the averaging interval is centered about $t = 1/4$, we are taking the inner product of the odd $\sigma_1(x, t)$ function and the even $\frac{\partial \dot{\gamma}}{\partial \sigma}(\sigma_0(t, y))$ function on the domain. In this case, the integral evaluates to zero.

Thus, to a first correction, a small amount of inertia gives the first correction term $\overline{\dot{\gamma}_1(t)} = 0$.

4 Experimental Results

The experimental setup has been explained in section 2.2. We used cornstarch suspensions of varying mass fractions between 52-55%. g_0 is maintained as the constant value of gravity. Theoretically, Δg increases with frequency as $\Delta g = (2\pi f)^2 A$. Between 1 ~ 20 Hz, acceleration generally increases with frequency. Between 20 ~ 25 Hz, however, the oscillation is more damped with the increase of frequency.

Between 1 ~ 14 Hz, the suspension develops Faraday waves when the volume controls were set sufficiently high. For low frequency 1 ~ 10 Hz, Faraday waves are stable and the suspension does not climb up after being finitely perturbed. For frequencies in the range of 12 ~ 14 Hz, Faraday waves are unstable to finite-amplitude perturbations, and the suspension can continuously climb up after being perturbed.

Between 12 ~ 19 Hz, columns of the suspension with thickness ~ 1 mm and width ~ 3 mm can climb up vertical surfaces. At frequencies greater than 20 Hz, however, such climbing motion is slowed down, possibly because our experimental setup lacks the power to maintain large accelerations at high frequencies.

Droplets of the dense suspension were formed on vertical surfaces via natural processes (e.g. “pinched off” from columns of the suspension and “splashing”) or by simply collecting a small amount of fluid and allowing it to wet the surface. At 53% mass fraction of cornstarch, droplets of thickness 1 ~ 2 mm are observed to climb up at 2mm/s under a sinusoidal signal of 15Hz, 100% volume, with an approximate $\Delta g \approx 89m/s^2$, $\Delta g/g_0 = 8.9$.

Holes and finger-like structures can appear between 14 ~ 25 Hz. At lower frequencies 14 ~ 19 Hz, the suspension quickly rises up as narrow finger-like structures. Its fluidity and instability can result in open and unstable holes on the surface of the suspension. At higher frequencies 20 ~ 25 Hz, the climbing motion has been reduced and the holes become more stable, as the finger-like structures are less mobile. This is possibly because the system is more jammed, or the oscillations are damped due to the mass of the platform and the fluid.

While most of the observed phenomena have been discussed in literature (e.g. Faraday waves, holes, and fingers [4][5]), climbing droplets have not been observed previously and are broadly consistent with both the “ratcheting” mechanism suggested by Deegan [10] and our generalization of the same to the notion of a “negative viscosity” effect.

5 Summary and Conclusions

The behavior of dense suspensions climbing up against oscillating gravity can be described in terms of an apparent “negative viscosity”, as average stress and shear rate are in opposite directions.

The Wyart-Cates (WC) model for dense suspensions is used to calculate shear rates and velocities. Average shear rates corresponding to oscillating stresses are first calculated. As with the “ratcheting” mechanism proposed in earlier work by Deegan, an apparent “negative viscosity” is only possible when the underlying flow curve exhibits DST or SJ: we find no such effect for fluids with CST. With DST and SJ fluids, we find that ϕ closer to ϕ_S and stress amplitudes $\Delta\sigma/\sigma > 1$ are of benefit to obtaining an apparent negative viscosity. Square wave forcing appears to be most efficient at exploring a fluid’s potential for climbing, since smoothly varying forcing protocols (e.g. sine-wave) are forced to spend more time exploring the non-inverted portion of the flow curve at positive shear rates, where large positive shear rates are sampled.

We believe that this basic “ratcheting” mechanism, or apparent “negative viscosity” effect, is relevant to a wide range of phenomena observed in VVDS. As a first generalization, we provided calculations of the WC model for a falling film under vibrating gravity. There, it was indeed found that the discussion on oscillating shear flows was directly relevant to explaining the conditions under which the net velocity of the film was opposed to the average influence of gravity.

Finally, as a proof-of-principle measure, we conducted experiments on VVDS that show fluid droplets steadily climbing up a vertically oriented surface. These climbing droplets are a new phenomenon in VVDS and, in our opinion, more cleanly isolate the mechanism behind a broader range of climbing behaviors documented in the literature. Again, it is our view that the motion of these droplets can be broadly interpreted in terms of simple concepts from the WC modeling framework.

In future studies, and as constitutive modeling capabilities for dense suspensions improve, it will be interesting to repeat this analysis to account for (for example) the effects of fluid reversal and non-local rheology. More accurate experimental measurements can also be done to more completely characterize the phenomena of “climbing droplets” in VVDS.

6 Acknowledgements

We thank Prof Mike Cates for the support and helpful discussions that made this project possible. Xingjian Hou thanks Dr Michal Kwasigroch and Dr Adam Boies for their guidance on research and funding. Work is funded by Trinity College Cambridge Projects Fund and DAMTP Soft Matter group.

References

- [1] M. Wyart and M. E. Cates, “Discontinuous shear thickening without inertia in dense non-brownian suspensions,” *Physical review letters*, vol. 112, no. 9, p. 098302, 2014.
- [2] C. Ness, R. Mari, and M. E. Cates, “Shaken and stirred: Random organization reduces viscosity and dissipation in granular suspensions,” *Science advances*, vol. 4, no. 3, p. eaar3296, 2018.
- [3] N. Y. Lin, C. Ness, M. E. Cates, J. Sun, and I. Cohen, “Tunable shear thickening in suspensions,” *Proceedings of the National Academy of Sciences*, vol. 113, no. 39, pp. 10774–10778, 2016.
- [4] F. S. Merkt, R. D. Deegan, D. I. Goldman, E. C. Rericha, and H. L. Swinney, “Persistent holes in a fluid,” *Phys. Rev. Lett.*, vol. 92, p. 184501, May 2004.
- [5] S. von Kann, J. H. Snoeijer, and D. van der Meer, “Phase diagram of vertically vibrated dense suspensions,” *Physics of Fluids*, vol. 26, no. 11, p. 113302, 2014.
- [6] T. Shinbrot, M. Rutala, A. Montessori, P. Prestininzi, and S. Succi, “Paradoxical ratcheting in cornstarch,” *Physics of Fluids*, vol. 27, no. 10, p. 103101, 2015.
- [7] A. Stephenson, “Xx. on induced stability,” *The London, Edinburgh, and Dublin Philosophical Magazine and Journal of Science*, vol. 15, no. 86, pp. 233–236, 1908.
- [8] R. Ramachandran and M. Nosonovsky, “Vibro-levitation and inverted pendulum: parametric resonance in vibrating droplets and soft materials,” *Soft Matter*, vol. 10, pp. 4633–4639, 2014.
- [9] P. Brunet, J. Eggers, and R. D. Deegan, “Vibration-induced climbing of drops,” *Phys. Rev. Lett.*, vol. 99, p. 144501, Oct 2007.

- [10] R. D. Deegan, “Stress hysteresis as the cause of persistent holes in particulate suspensions,” *Phys. Rev. E*, vol. 81, p. 036319, Mar 2010.
- [11] J. J. J. Gillissen, C. Ness, J. D. Peterson, H. J. Wilson, and M. E. Cates, “Constitutive model for shear-thickening suspensions: Predictions for steady shear with superposed transverse oscillations,” *Journal of Rheology*, vol. 64, no. 2, pp. 353–365, 2020.
- [12] I. M. Krieger and T. J. Dougherty, “A mechanism for non-newtonian flow in suspensions of rigid spheres,” *Transactions of the Society of Rheology*, vol. 3, no. 1, pp. 137–152, 1959.
- [13] T. P. Szynalski, “Online tone generator.” <https://www.szynalski.com/tone-generator/>. [Online; accessed 10-Sep-2021].